

Emission From Rotation-Powered Pulsars: Is It All Relative?

Alice K. Harding

NASA Goddard Space Flight Center, Greenbelt, MD 20771, USA

Thirty-five years after the discovery of rotation-powered pulsars, we still do not understand the fundamentals of their pulsed emission at any wavelength. Even detailed pulse profiles cannot identify the location of the emission in a magnetosphere that extends from the neutron star surface to near the light cylinder. Compounding the problem are effects of strong gravity at low altitudes and plasma moving at relativistic speeds in the outer magnetosphere. I will discuss the role of special and general relativistic effects on pulsar emission, from inertial frame-dragging near the stellar surface to aberration, time-of-flight and retardation of the magnetic field near the light cylinder. Understanding how these effects determine what we observe at different wavelengths is critical to unraveling the emission physics

1. INTRODUCTION

Rotation-powered pulsars shine over a broad spectrum from radio to high-energy γ -ray wavelengths. Pulsed emission in the radio band, where they were first discovered, has been detected from over 1500 objects and the characteristics of this emission have been studied in great detail for many years. Even so, the origin of the radio pulsation is still not understood, except to realize that it must be a coherent process requiring significant particle densities and probably electron-positron pairs [29]. Studies of radio pulse morphology and phase-resolved polarization patterns suggest that the emission is radiated along open dipole magnetic field lines within several hundred stellar radii of the polar cap [26, 39]. Pulsed emission in optical, X-ray and γ -ray bands has been detected from a much smaller number of sources. Some thirty pulsars are known to have pulsations at X-ray energies [23], ten in the optical band [31] and about ten at γ -ray energies [22]. Since emission at the higher energies originates from incoherent processes, there is greater hope of understanding its origin, as well as the particle acceleration processes in the magnetosphere. But nature seems to be making things difficult for us here as well, as in most cases the high-energy pulse profiles do not look like the radio profiles and the phases of the pulses are different across energy bands. There are, however, notable exceptions to this behavior. The Crab pulsar exhibits a double-peaked pulse profile that is very similar at all wavelengths from radio to high-energy γ rays, and the pulses are in phase across the entire spectrum to within tenths of milliseconds [27]. Several other pulsars with comparably short or shorter pulse periods show similar behavior, having X-ray and radio profiles that resemble each other and are in phase. These sources include PSR B0540-69, a 50 ms Crab-like pulsar in the LMC, PSR J1617-5055, a 69 ms pulsar in RCW103, and the millisecond pulsars PSR B1821-24, PSR J0437-4715 and PSR B1937+21. Perhaps this indicates that the emission at these different wavelengths originates in the same small region of the magnetosphere. However, there is another possi-

bility if one takes into account relativistic effects on emission, and which may agree better with emission models as well as constraints on viewing angles and polarization measurements.

The key to deciphering pulsar emission, I believe, is to understand the relativistic effects that operate near a rapidly spinning, magnetized star with strong gravity, to build these into our models, and to recognize how they distort the radiation we observe. If we can learn to deconvolve these effects from the signals, or to identify signatures which can give us information on the location of the emission, then perhaps we will have clues to the acceleration and emission mechanisms. Special relativistic effects such as aberration, time-of-flight delays and retardation of the magnetic field become important for acceleration and radiation in the outer magnetosphere. General relativistic effects such as inertial frame-dragging, gravitational red-shift and light bending are important nearer the neutron star surface. I will review these special and general relativistic effects in pulsar magnetospheres, how they are being incorporated into pulse emission models and how they are essential to accurately interpreting pulsar data to determine the geometry of the emission.

2. SPECIAL RELATIVISTIC EFFECTS

Pulsars rotate rapidly enough that the star's exterior magnetic field and charges that are coupled to it will experience relativistic corotation velocities in the outer parts of the magnetosphere. Since the corotation velocity at radius r , for angle ζ to the rotation axis, is $\beta_{rot} = \Omega r \sin \zeta / c$, first order special relativistic effects become important when r is a significant fraction of the light cylinder radius, $R_{LC} = c/\Omega$, where Ω is the pulsar rotation frequency. Aberration causes the photon emission directions to appear shifted to a non-rotating observer in the direction of rotation, so the emission arrives at an earlier phase. The first order phase shift due to aberration, at an emission

arXiv:astro-ph/0503300v1 14 Mar 2005

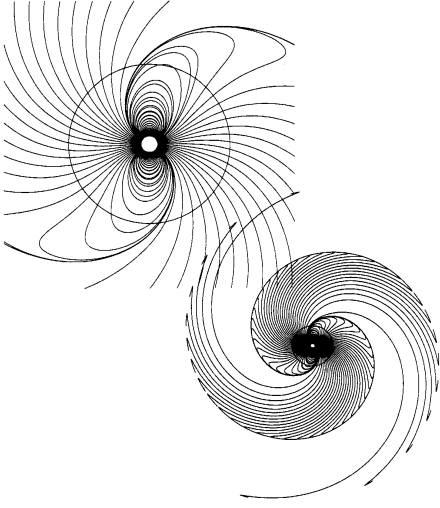


Figure 1: Sweepback of the vacuum dipole magnetic field in the spin-equatorial plane (from [49]) for pulsar inclination angle is 60° . Rotation is counterclockwise and the circle denotes the light cylinder radius. Top view shows inside and just outside the light cylinder and bottom view shows the field forming a spiral pattern far outside the light cylinder.

radius r_{em} , is [13, 14]

$$\Delta\phi_{\text{ab}} \simeq -\frac{r_{\text{em}}}{R_{\text{LC}}}, \quad (1)$$

which is independent of the angle ζ . In addition, there are time-of-flight delays in the arrival time of radiation emitted at different r_{em} . The phase delay is, to first order in β_{rot} , the same as that due to aberration, or

$$\Delta\phi_{\text{ret}} \approx -\frac{r_{\text{em}}}{R_{\text{LC}}}. \quad (2)$$

The magnetic field of the neutron star will be distorted by retardation in the outer parts of the magnetosphere near the light cylinder. The original Deutsch [8] solution for a rotating dipole field in vacuum exhibits such an effect, as the ‘near field’ dipole must match to the ‘far-field’ electromagnetic wave solution. Beyond the light cylinder the field lines become swept back, in the opposite direction to that of rotation (see Figure 1). However, the field begins to be distorted within the magnetosphere, and this can affect both the direction of emission tangent to field lines as well as the shape of the open field volume [1, 49]. The lowest order change in the field direction caused by the sweep-back inside the light cylinder is [43]

$$\delta_{\text{sb}} \simeq 1.2 \left(\frac{r_{\text{em}}}{R_{\text{LC}}} \right)^3 \sin^2 \alpha, \quad (3)$$

where α is the magnetic inclination angle, which is insignificant compared with the phase shifts due to aberration and time-of-flight. There is however a much more important distortion of the open field volume, due to field-line sweep-back near the light cylinder, which results in distortion and displacement of the polar cap at the surface of the neutron star. The displacement of the open field volume causes a phase shift [9]

$$\Delta\phi_{\text{ov}} \simeq 0.2 \left(\frac{r_{\text{em}}}{R_{\text{LC}}} \right)^{1/2} \quad (4)$$

which is of lower order than aberration and time-of-flight delay and thus will dominate at smaller emission radii. The retarded vacuum dipole solution has been widely used in modeling pulsar emission [6, 42, 43], even though active pulsar magnetospheres will contain charges and currents, because solutions for the realistic case are more complex and model dependent. An analytic solution for a pulsar magnetosphere with currents on open field lines in a space-charge limited flow (SCLF) model [35] illustrates that there are important differences in the vacuum and non-vacuum cases. For example, there is no sweepback of field lines for an aligned rotator in the vacuum case (where there is no spin-down torque) but there *is* sweepback in the case of the non-vacuum aligned rotator due to the current flow.

2.1. GENERAL RELATIVISTIC EFFECTS

Distortions of space-time near the neutron star produce various effects important to pulsar radiation, including gravitational red-shifting of photons, bending of light, curved space-time changes to the magnetic field and inertial frame-dragging. The frequency of radiation emitted near the neutron star surface is red-shifted as photons climb out of the gravitational potential well toward a distant observer in the (relatively) flat space-time of Earth’s gravity. The resulting decrease in energy of the photons emitted at radius r_{em} is

$$\varepsilon = \varepsilon' \left(1 - \frac{2GM}{r_{\text{em}}c^2} \right)^{1/2}. \quad (5)$$

Such a red-shift can also have secondary effects on the radiation, such as an increased efficiency of attenuation by one-photon pair creation [15] and photon splitting [4], since these processes depend sensitively on photon energy.

Gravitational bending of photon paths is most pronounced for trajectories at large angles to the radial direction. For non-thermal radiation by highly relativistic particles that is emitted mostly tangent to magnetic dipole field lines in polar regions, light bending has a second-order effect on radiation direction

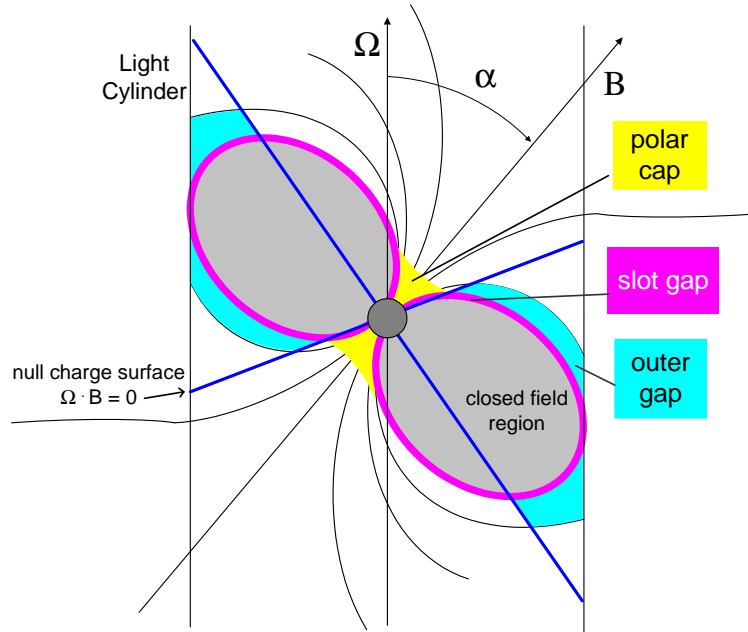


Figure 2: Schematic illustration of pulsar acceleration/emission models.

and attenuation. However, for thermal emission from a hot neutron star surface, emitted semi-isotropically, light bending has a dominant effect on smearing-out pulse profiles and diminishing degree of modulation [37, 40].

The dipole field in a Schwarzschild metric [48] exhibits several features that are important for pulsar radiation. The surface field strength at the magnetic poles is increased, relative to flat space-time, so that

$$B_0^{GR} \approx \left(1 + \frac{r_g}{R}\right) B_0^{Flat} \quad (6)$$

where R is the radius and r_g is the gravitational radius of the neutron star. This effect also enhances the photon attenuation due to pair creation and photon splitting. The dipole field is also less open, as field lines near the light cylinder have footpoints that are nearer the magnetic axis. There is a resulting decrease in polar cap half-angle,

$$\theta_{GR} \approx \frac{\theta_{Flat}}{\sqrt{1 + r_g/R}}. \quad (7)$$

Effectively though, for emission of photons tangent to field lines, the effect of light bending tends to cancel the effect of the smaller polar cap size, so that the resulting size of the emission beam is roughly the same as in flat space-time [15].

The fast rotation of the neutron star also distorts the nearby space-time, resulting in a dragging of the

inertial frame around it (also known as the Lense-Thirring effect). In the Kerr metric that includes the rotation of the neutron star, the inertial frame rotates with angular velocity, $\omega = 2GL/c^2r^3$, if L is the neutron star angular momentum, which is effectively a differential rotation. If one solves Maxwell's equations in this metric to obtain the electric field induced by the rotation of the magnetic field [36], there is a correction to the Goldreich-Julian charge density (the charge density required to screen the electric field parallel to the magnetic field),

$$\rho_{GJ} \approx -\frac{1}{4\pi c} \nabla \cdot \left[\frac{1}{\alpha} (\mathbf{v} - \boldsymbol{\omega}) \times \mathbf{B} \right], \quad (8)$$

where $\mathbf{v} = \boldsymbol{\Omega} \times \mathbf{r}$. The inertial-frame angular velocity now appears in the expression for ρ_{GJ} , as well as the rotational velocity \mathbf{v} . This change in ρ_{GJ} turns out to have a significant effect for SCLF models [2], where the accelerating electric field results from the small difference between the actual charge flow along the open field lines and the GJ charge flow,

$$\nabla \cdot E_{\parallel} = 4\pi(\rho - \rho_{GJ})$$

The resulting parallel electric field near the neutron star is 10 to 50 times higher than the corresponding field in flat space-time (MT92), so that the frame-dragging contribution actually dominates. The frame-dragging E_{\parallel} also enables particle acceleration for aligned rotators and along field lines curving away

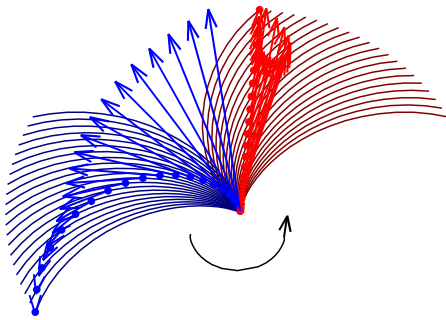


Figure 3: Time-lapse illustration of formation of caustic emission in the spin-equatorial plane of an orthogonal rotator. The magnetic axis is vertical at time $t = 0$ and rotates counterclockwise. Dots and arrows mark the successive emission points and directions of photons along the leading and trailing last open field lines that will arrive at a distant observer simultaneously.

from the rotation axis, which does not occur in flat space-time.

3. DECODING THE SIGNALS

Many of the effects described above have been incorporated in pulsar emission models and in some cases, they are essential features. Most current models for high energy emission involve some particle acceleration and radiation in the outer magnetosphere. Although traditional polar cap models [7, 17] focus on activity near the neutron star, more recently such models have explored extended acceleration from the neutron star surface to high altitudes in the slot gap along the edge of the open field region [34] (see Figure 2). Acceleration in outer gap models [6, 20, 42] occurs in the outer magnetosphere between the null charge surface and the light cylinder along the last open field line, although recent 2D solutions of the gap geometry show that the gap may extend to the inner magnetosphere [45]. Polar cap and outer gap model geometry thus seems to be merging, although the electrodynamics of the two models remains fundamentally different. In both pictures, special relativistic effects are essential in modeling the high altitude emission. General relativistic effects are additionally important in polar cap models.

3.1. Caustics

A curious feature of the emission pattern in the outer magnetosphere of a rotating dipole was first noted by Morini [32]. If one assumes that photons are radiated tangent to the magnetic field from the polar

cap to the light cylinder, then the relative phase shifts of photons emitted at different radii due to dipole curvature, aberration and time-of-flight nearly cancel on field lines on the trailing edge of the open region (see Figure 3). Radiation along such trailing field lines bunches in phase, forming a sharp peak in the profile. On the other hand, photons emitted at different radii along leading field lines spreads out in phase. The effect is most pronounced for large inclination of the magnetic axis to the rotation axis. A plot of observer angle to the rotation axis versus phase, as shown in Figure 4a, clearly displays the sharp lines of emission, or caustics, in the radiation from trailing field lines. A number of emission models [5, 12, 42, 44] have made use of the caustic effect to produce the sharp peaks seen in profiles of high-energy pulsars. In purely geometrical schemes, the high energy emission could originate from caustics associated with either one magnetic pole [32, 42, 44], or both poles [12]. Two types of physical acceleration and emission models divide in this way as well, with outer gap models exhibiting one-pole caustic geometry and slot gap models exhibiting two-pole caustics.

3.2. Outer Gap Model

Outer-gap models [5, 41] assume that acceleration occurs in vacuum gaps that develop in the outer magnetosphere, along the last open field line above the null charge surfaces, where the Goldreich-Julian charge density changes sign (see Figure 2), and that high-energy emission results from photon-photon pair production-induced cascades. The pair cascades screen the accelerating electric field and limit the size of the gap both along and across the magnetic field. The geometry of the outer gaps prevents an observer from seeing gaps associated with both magnetic poles, putting them in the class of one-pole caustic models. The high energy pulse profiles that are observed to have two widely separated, sharp peaks are formed by caustics, the leading peak originating from overlapping field lines at $r_{\text{em}} \sim 0.9 R_{LC}$ and the trailing peak originating from the caustic along trailing field lines at $r_{\text{em}} \sim 0.2 - 0.8 R_{LC}$. An example of outer gap profile formation is shown in Figure 4c and 4d. A drawback to this type of model is that the formation of the leading peak is very sensitive to the structure of the retarded field lines very near the light cylinder, which is not well known for non-vacuum models (see Section 2). Some recent outer gap models point out that the gap lower boundary should exist somewhat below the null charge surface, and the location of this boundary will depend on the external currents that flow into or out of the gap [21, 45]. If the gap moves close enough to the neutron star, depending on inclination angle, it might be possible for an observer to see gaps from both magnetic poles.

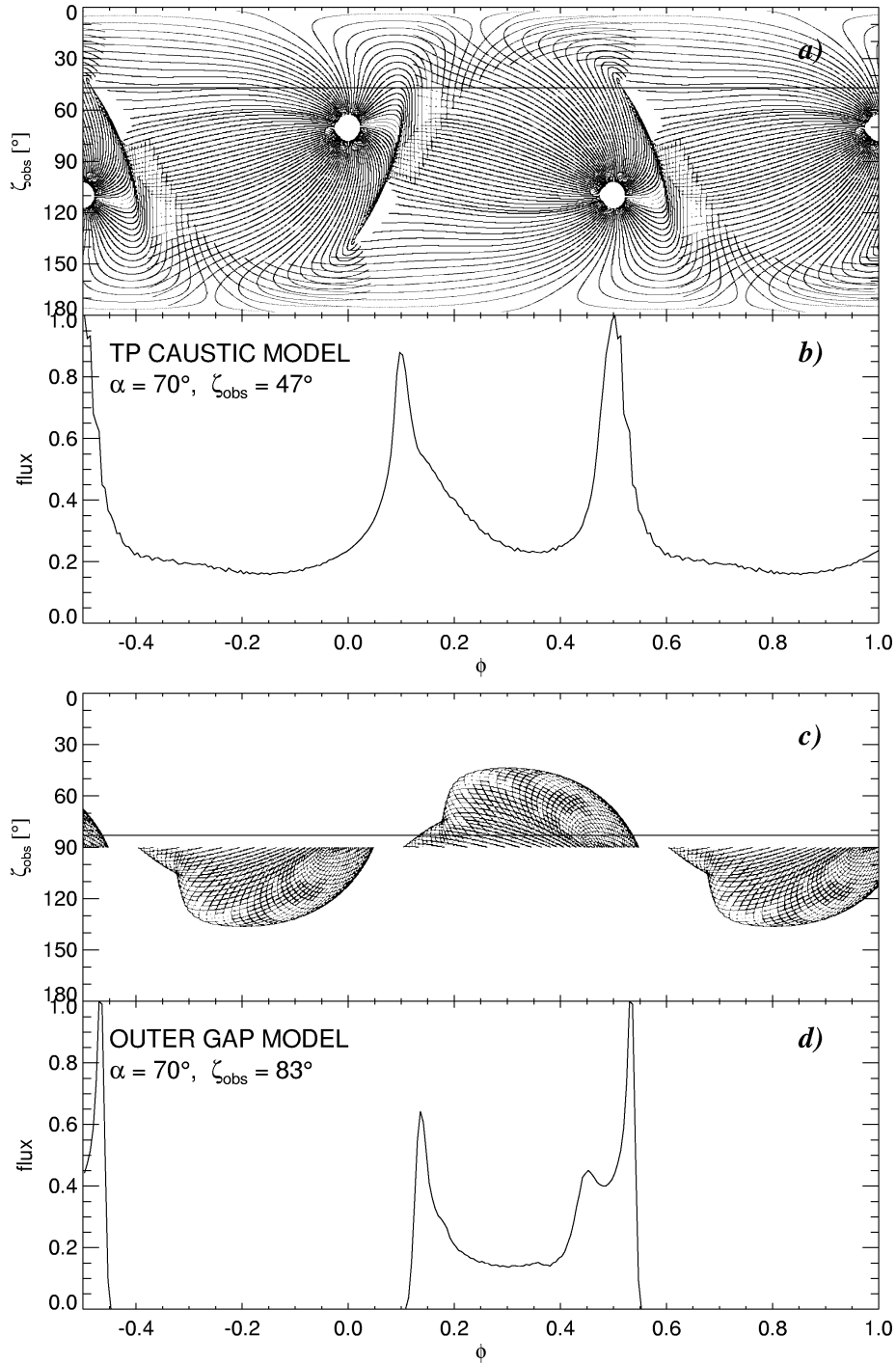


Figure 4: Comparison of two-pole caustic and outer gap models. a) Plot of emission in the $(\zeta_{\text{obs}}, \phi)$ plane, calculated with a two-pole caustic model for inclination, $\alpha = 70^\circ$. ϕ is the rotational phase and ζ_{obs} is the viewing angle measured from the rotation axis. b) High-energy profile for $\zeta_{\text{obs}} = 47^\circ$, produced by a horizontal cut through the phase plot above. c) As in a) for an outer gap model. d) High-energy profile from the outer gap phase plot c) for $\zeta_{\text{obs}} = 83^\circ$.

3.3. Slot Gap Model

The slot gap, a narrow pair-free accelerator bordering the closed field region, is a feature of polar cap SCLF models (AS79). SCLF models assume freely

emitted charges flow out from the neutron polar cap along open field lines. Since this charge flow is not sufficient to supply the Goldreich-Julian charge above the surface, as discussed in Section 2.1, an E_{\parallel} exists and charges are accelerated. Radiation from these charges

forms electron-positron pairs in the strong magnetic field, which can screen the E_{\parallel} above a pair front in a distance small compared to the acceleration distance. These models assume a boundary condition that the accelerating electric field and potential vanish at the last open field line. Near the boundary, the electric field is decreasing and a larger distance is required for the electrons to accelerate to the Lorentz factor needed to radiate photons energetic enough to produce pairs. The pair front thus occurs at higher and higher altitudes as the boundary is approached and curves upward, becoming asymptotically parallel to the last open field line. Since E_{\parallel} is unscreened in the slot gap, particles continue to accelerate and radiate to high altitude along the last open field lines. It is interesting that frame-dragging's dominant effect on the accelerating field persists even at large distances from the neutron star surface, since the high-altitude SCLF solution depends on surface boundary conditions [34]. The resulting emission geometry naturally creates caustics visible from both poles, and so produces double-peaked pulse profiles similar to the two-pole caustic model of Dyks & Rudak [12], as shown in Figures 4a and 4b. In contrast to one-pole outer gap models, slot gap models have outward emission beams below the null-charge surface. Both peaks originate from trailing field-line caustics at intermediate radii $r_{\text{em}} \sim 0.1 - 0.7 R_{LC}$. In such profiles, the leading 'outer gap' peak appears as a bump just following the first peak.

3.4. Comparing Outer Gap and Slot Gap Models

Although outer gap and slot gap models can produce similar pulse profiles, phase plots of their emission show prominent differences. As displayed in Figure 4a, slot gap emission fills the entire sky even though radiation is produced only on field lines bordering the closed regions. Since the radiation is emitted over the entire length of these field lines from the magnetic poles (the hollow circles in Fig. 4a) to near the light cylinder (where field lines from opposite hemispheres overlap), observers can view the emission from both magnetic poles at a wide range of angles. Two-pole caustic emission can be seen for inclination angles $\alpha \gtrsim 30^\circ$ [10]. Because the emission fills the sky, radiation will be visible at all pulse phases so that pulse profiles like the one shown in Figure 4b will include 'off-pulse' emission. The bump or shoulder appearing on the inside of the first peak is due to emission from overlapping field lines from opposite poles, and occurs at the same phase as the first peak in outer gap models. It is interesting that the γ -ray profile of the Vela pulsar displays a similar broad bump [22].

Outer gap emission fills only a fraction of the sky,

as shown in Figure 4c, since outward-going radiation occurs only above the null charge surface in each hemisphere. The outer gap emission pattern is thus a subset of the two-pole caustic emission pattern. In Figure 4c, the magnetic poles are not visible and part of the caustic near each pole is cut off. The pattern fills the most phase space for large inclination angles, but shrinks to a small area near the rotational equator for small inclination [6]. Outer gap emission is never visible at small viewing angles $\zeta_{\text{obs}} \lesssim 30^\circ$ at any inclination angle. An observer cutting through the pattern at a single ζ_{obs} will see emission only from field lines originating at one pole. As a result, the peaks in outer gap profiles drop sharply at their outer edges and there is no off-pulse emission outside the peaks, as is evident in Figure 4d. The second peak has the same origin as the second peak in the two-pole caustic model, but the first peak is formed by emission from overlapping field lines very near the light cylinder (similar to the formation of the bump in Figure 4b).

4. DETECTING THE SIGNATURES

Emission models can make predictions of certain observable signatures, which may provide clues to both the relativistic effects that are shaping radiation patterns and to the location and nature of the radiation. Such signatures are found in the relative phases of emission at different wavelengths, the polarization patterns and the spectrum of radiation.

4.1. Phase Shifts

Multiwavelength behavior of observed pulse profiles contains a wealth of information, but has proven to be extremely complex and difficult to interpret. With detailed modeling of emission, taking into account effects of rotation and strong gravity of the neutron star, we can possibly understand why many of the short period pulsars have pulse profiles that show phase coherence of emission at different wavelengths while longer period pulsars do not. For example, as discussed in Section 3.1, caustic emission along trailing field lines puts emission radiated over a large range of different altitudes in phase for a distant observer. This means that any radiation originating between $r_{\text{em}} \sim 0.1 R_{LC}$ and $r_{\text{em}} \sim 0.8 R_{LC}$ near the last open field line will appear in phase, but radiation originating outside this region will appear at different phases. This feature of caustics may offer an explanation of multiwavelength phase coherence seen in the profiles of fast pulsars. The altitude of caustic formation is the same fraction of light cylinder radius in all pulsars, independent of period. However, emission at various wavelengths in different pulsars may not all originate within the radii

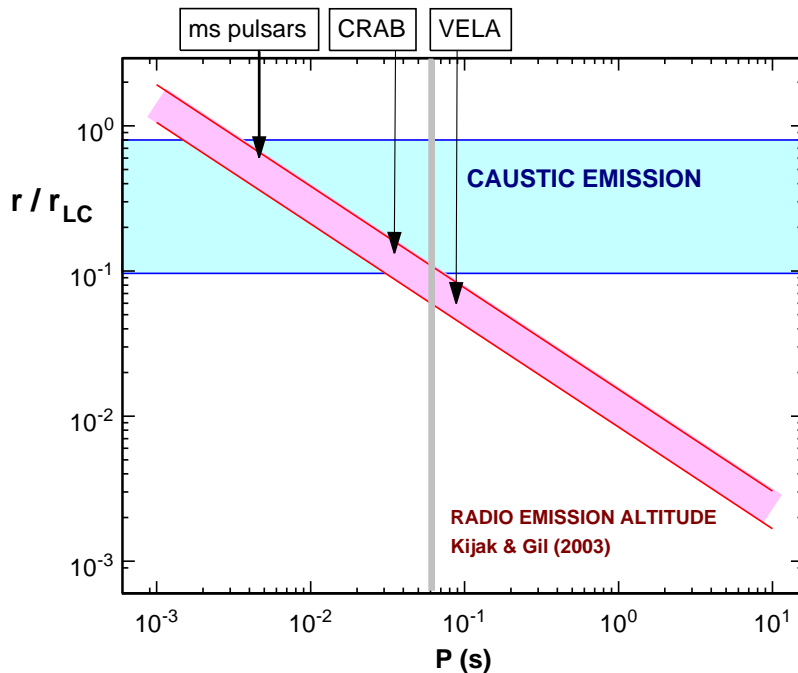


Figure 5: Radio emission radius (in units of light cylinder radius) as a function of pulsar period from [26]. Also shown is the range of radii there caustic emission occurs.

of caustic formation. To illustrate this point, Figure 5 displays the dependence of pulsar radio emission altitude as a function of pulse period, determined empirically from observed pulse widths and radius-to-frequency mapping [26], superposed on the altitude range of caustic formation. Although the exact altitudes of pulsar radio emission are not necessarily known this well, there is indication of such a dependence on period. In that case, it can be seen that radio emission will originate within the caustic formation region only for the fastest pulsars. The pattern of radio conal emission, that may originate near the last open field lines, will then become severely distorted into caustic emission peaks. In this example, the dividing point occurs around a period of 60 ms, so that radio and high-energy emission would be phase coherent for the Crab and most millisecond pulsars, but not for Vela and pulsars with longer periods. This in fact seems to match observation. The radio emission in slower pulsars in this picture occurs at altitudes below the caustic region, so that the observer light-of-sight would cross the radio core and/or conal beams close to the magnetic pole before crossing the high energy caustics.

Another example of relativistic effects that cause phase-shift signatures in pulsar emission occurs in observed radio profiles. In pulsars with both core and one or more conal beams (i.e. profiles containing three or five peaks), there is often a phase shift between the central core component and the center of the profile as

determined by the conal beam(s). In most cases, the conal components lead the core component in phase. Such phase shifts have been interpreted as due to a combination of aberration (Eqn 1) and time delay (Eqn 2) if the conal emission occurs at a higher altitude than the core emission [14]. Shifts in the center of the polarization position angle curve are also observed and could be caused by the same effects [3]. There are some pulsars whose radio profiles show phase shifts in the opposite direction (the conal components lag the core components). This may be due to a dominating phase shift caused by the distortion of the open field volume due to sweepback of the magnetic field [9] (Eqn. 4). Such phase shift in radio profiles have been used to derive the radio emission altitudes and they generally agree with those derived by other methods [13].

4.2. Polarization

Phase-resolved polarimetry of pulsar emission has proven to be a powerful diagnostic at radio wavelengths. The pulsed non-thermal radiation from relativistic particles in the magnetosphere is tightly beamed along the neutron-star magnetic field lines and thus the emitted radiation is believed to be highly polarized either parallel or perpendicular to the field lines. Measurement of the polarization properties as a function of pulse phase can provide a multidimensional mapping of the field pattern at the emission

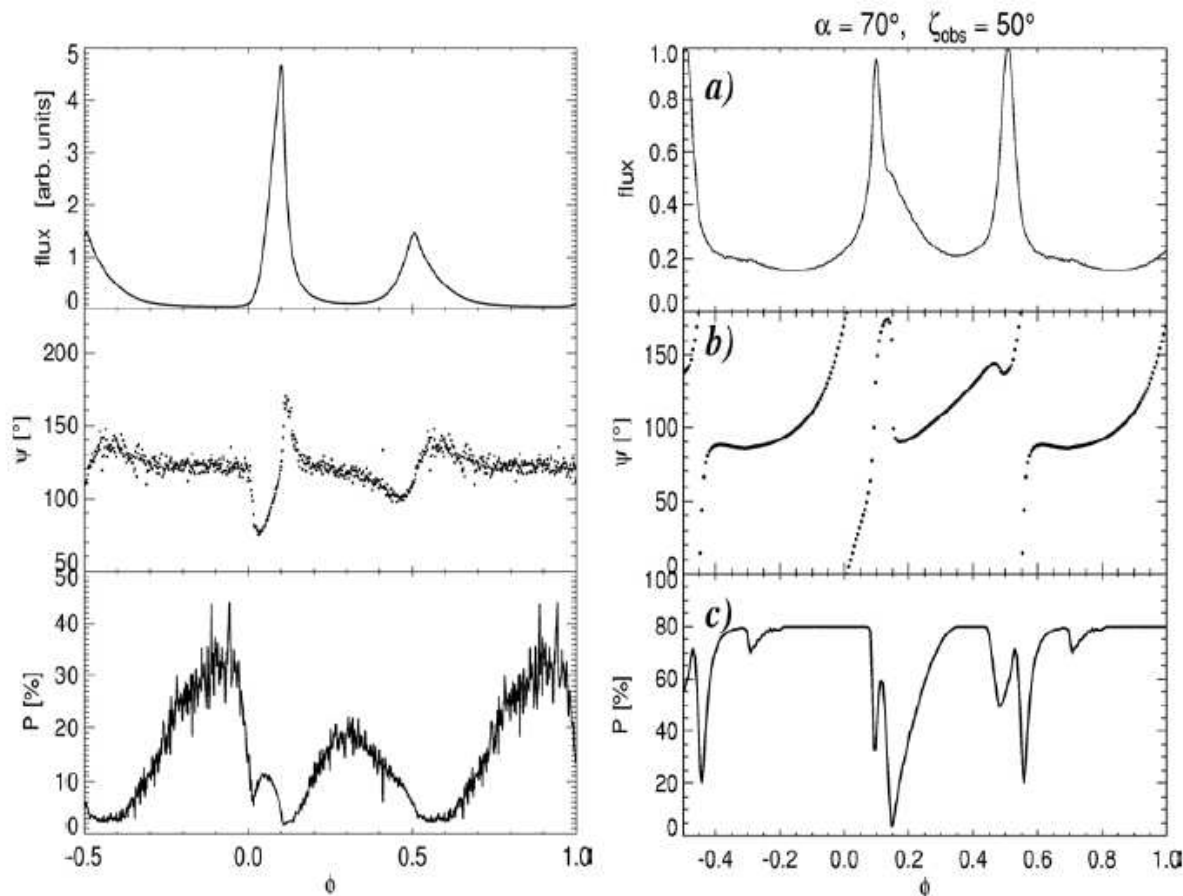


Figure 6: Left: Optical profile (top), polarization position angle Ψ (middle) and degree of polarization (bottom) of the Crab pulsar from OPTIMA [24]. Right: Model profile and polarization characteristics predicted by a two-pole caustic model [10] with dipole inclination $\alpha = 70^\circ$ and viewing angle $\zeta_{\text{obs}} = 50^\circ$. The PA curve has 180° wraparound ambiguity.

sites. In the classical rotating vector model (RVM) [38], the expected signature of emission near the poles of a dipole field, an ‘S’-shaped swing of the polarization position angle through the pulse profile, has been seen from many radio pulsars and has generally been taken as proof that the radio emission originates from the open field lines of a magnetic dipole. However, while this classical picture can provide a good measurement of the observer angle with respect to the magnetic pole, β , for low-altitude emission, it does not provide an unambiguous measure of pulsar inclination angle α . Furthermore, if the emission occurs at altitudes that are more than a few tenths of the light cylinder radius, relativistic effects can significantly distort the simple polarization characteristics predicted by the classical model. But such distortions can be turned to our advantage if we can model them well enough to understand the signatures of the effects.

As discussed in Section 4.1, one would expect severe distortion of emission patterns by special relativistic effects for radiation originating within the caustic emission region shown in Figure 5. The emission from fast pulsars would thus be more likely to show signatures of such effects in their polarization patterns, especially at high energies. It would be very important to have polarization data at high energies to explore characteristics of emission in the outer magnetosphere. Unfortunately, polarization measurements at wavelengths other than radio exist for very few pulsars. In the case of the Crab pulsar, polarization measurements have been made at radio and optical wavelengths and do not show the simple shape predicted by the classical RVM. As shown in Figure 6, each peak shows a very sharp swing of position angle (PA) and a drop in degree of polarization. Such PA swings could be interpreted as part of an S-curve for small impact angle β , but then one would expect

a peak separation of 180° (rather than the 140° observed) in a 2-pole, near-surface emission model, and no drop in degree of polarization. Figure 6 also shows a computed pulse profile, PA curve and degree of polarization as a function of phase predicted in a 2-pole caustic model [10], described in Section 3.1. Sharp swings of PA and drops in degree of polarization are signatures of caustic emission and the qualitative similarity of the observed and model polarization characteristics seem to strengthen the case for caustic peaks in the Crab pulsar. This picture is also consistent with the mutliwavelength phase coherence property expected for fast pulsars, discussed in Section 4.1.

Optical polarization measurements have recently been made [25] for the slower 384 ms pulsar PSR B0656+14. The double-peaked optical profile is not in phase with the single radio peak, but the classical RVM provides a consistent fit of both radio and optical PA data. One interpretation of these results is that both radio and optical emission from this middle-aged pulsar originate at low altitudes, with the high-energy emission described by a hollow-cone centered on the magnetic pole and the radio core emission, as predicted by the traditional polar cap model [7].

4.3. Spectra

Spectral signatures can also provide clues to emission altitudes as well as some relativistic effects. Polar cap [7] and slot gap [33] models include a component of emission from low-altitude pair cascades. The observable spectra of the cascade emission will exhibit sharp high-energy cutoffs due to pair attenuation, at an energy of approximately [4]

$$E_c \sim 2 \text{ GeV } P^{1/2} \left(\frac{r}{R} \right)^{1/2} \max \left\{ 0.1, B_{0,12}^{-1} \left(\frac{r}{R} \right)^3 \right\} \quad (9)$$

where $B_{0,12}$ is the surface magnetic field in units of 10^{12} , r is the emission radius and R is the neutron star radius. Such cutoffs could be identified by their super-exponential shape, and distinguishable from the simple exponential cutoffs due to a maximum in the radiating particle spectrum. The detection of a pair attenuation cutoff would require the emission region to be located in the strong magnetic field within several stellar radii of the neutron star surface. Dyks & Rudak [11] have shown that even at relatively low altitudes, aberration and field-line slippage cause by neutron star rotation can produce asymmetries in pair production cutoffs across the polar cap, such that spectra radiated on leading-edge field lines are cut off at lower energies than are spectra radiated on trailing-edge field lines. This produces an asymmetry in the pulse profile, as the trailing peak will dominate at energies approaching the cutoff and the first peak will disappear. In fact, in the double-peaked profiles of three bright γ -ray pulsars observed by *EGRET*, the

Crab, Vela and Geminga, the trailing peak dominates above 5 GeV [46].

It has been suggested [47] that the high-energy γ -ray spectra of millisecond pulsars may provide constraints on the frame-dragging electric field, discussed in Section 2.1. Since the electric fields near the surface of millisecond pulsars are expected to be unscreened, due to insufficient pair production in their very low magnetic fields, the peak of their high-energy curvature radiation spectrum, predicted to be at 1 – 50 GeV, should be a sensitive measure of E_{\parallel} [18]. Non-detection of the nearby millisecond pulsar PSR J0437-4715 by *EGRET* already places marginal constraints on the neutron star equation-of-state dependence in the frame-dragging acceleration model [16], and future observations by air-Cherenkov telescopes will place further constraints.

5. FUTURE PROSPECTS

Future measurements by high-energy telescopes that have recently begun operations or are soon to come will be capable of detecting or significantly constraining most of the signatures that have been discussed here. The *Gamma-Ray Large Area Space Telescope (GLAST)* [30], with expected launch in 2007, will have the sensitivity to detect γ -ray emission between 30 MeV and 300 GeV from possibly several hundred pulsars. *GLAST* should easily detect nearby millisecond pulsars like PSR J0437-4715, thereby putting severe constraints on frame-dragging acceleration models. Measurement of pulse profiles of many pulsars of varying ages and periods, and comparison with their radio profiles, can test the predictions of outer gap and slot gap caustic models. New air-Cherenkov telescopes such as *MAGIC* [28] and *H.E.S.S.* [19] are expected to achieve sensitivity below 100 GeV and may detect, or at least place further limits on, millisecond pulsar spectra. *INTEGRAL* and *RHESSI* currently have some sensitivity to polarized signals at 100-500 keV and > 20 keV, but not enough for the phase-resolved polarimetry required to detect signatures of caustic emission in pulsars. Several proposed X-ray polarimeters are currently under study, the *Advanced X-Ray Polarimeter (AXP)* and the *Polarized Gamma-Ray Observer (PoGO)*, sensitive from 2-10 keV and 25-200 keV respectively. Such detectors are expected to have enough sensitivity to distinguish between the different emission models and to detect caustic signatures in the Crab pulsar.

References

- [1] P. N. Arendt & J. A. Eilek, ApJ, submitted, 1998 (astro-ph/98011257).
- [2] J. Arons & E. T. Scharlemann, ApJ, 231, 854, 1979.
- [3] M. Blaskiewicz, J. M. Cordes, I. Wasserman, ApJ, 370, 643, 1991.
- [4] M. G. Baring & A. K. Harding ApJ, 547, 929, 2001.
- [5] K. S. Cheng, C. Ho, & M. A. Ruderman, ApJ, 300, 500, 1986.
- [6] K. S. Cheng, M. A. Ruderman & L. Zhang, ApJ, 537, 964, 2000.
- [7] J. K. Daugherty & A. K. Harding, ApJ, 458, 278, 1996.
- [8] A. Deutsch, Annales d'Astrophysique, 18, 1, 1955.
- [9] J. Dyks & A. K. Harding, ApJ, 614, 869, 2004.
- [10] J. Dyks, A. K. Harding & B. Rudak, ApJ, 606, 1125, 2004.
- [11] J. Dyks & B. Rudak, A & A, 393, 511, 2002.
- [12] J. Dyks & B. Rudak, ApJ, 598, 1201, 2003.
- [13] J. Dyks, B. Rudak & A. K. Harding, ApJ, 607, 939, 2004.
- [14] R. T. Gangadhara & Y. Gupta, ApJ, 555, 31, 2001.
- [15] P. L. Gonthier & A. K. Harding, ApJ, 425, 747, 1994.
- [16] A. K. Harding, in "Symposium on High Energy Gamma-Ray Astronomy", ed. F.A. Aharonian and H. Voelk (AIP) in press, 2005.
- [17] A. K. Harding & A. G. Muslimov, ApJ, 508, 328, 1998.
- [18] Harding, A. K., Usov, V. V. & Muslimov, A. G., ApJ, in press, 2005.
- [19] J. A. Hinton et al., New Astron.Rev., 48, 331, 2004.
- [20] K. Hirotani & S. Shibata, MNRAS, 325, 1228, 2001.
- [21] K. Hirotani, A. K. Harding & S. Shibata, ApJ, 591, 334, 2003.
- [22] G. Kanbach, in "Neutron Stars, Pulsars, and Supernova Remnants", ed. W. Becker and H. Lesch, and J. Trmper (Max-Planck-Institut fr extraterrestrische Physik: Garching bei Mnchen), 91, 2002.
- [23] V. M. Kaspi, M. S. E. Roberts & A. K. Harding, in "Compact Stellar X-Ray Sources", ed. W. H. G. Lewin & M. van der Klis (Cambridge Univ. Press), in press (astro-ph/0402135).
- [24] S. Kellner, 2002, Diplomarbeit, Technische Univ. Munchen.
- [25] B. Kern, C. Martin, B. Mazin & J. P. Halpern, ApJ, 597, 1049, 2003.
- [26] J. Kijak & J. Gil, A & A, 397, 969, 2003.
- [27] Kuiper, L.; Hermsen, W.; Walter, R.; Foschini, L. 2003, A & A, 411, 31.
- [28] E. Lorenz, New Astron. Rev., 48, 339, 2004.
- [29] D. B. Melrose, in "Pulsar Astronomy - 2000 and Beyond", IAU Coll. 177, ed. M. Kramer, N. Wex & Wielebinski (San Francisco:ASP), 721, 2000.
- [30] J. E. McEnery, I. V. Moskalenko, & J. F. Ormes, to appear in "Cosmic Gamma Ray Sources", Kluwer ASSL Series, Edited by K.S. Cheng and G.E. Romero, 2004.
- [31] R. P. Mignani, A. DeLuca & P. A. Caraveo, in "Young Neutron Stars and Their Environments" (IAU Symposium 218, ASP Conference Proceedings), eds F. Camilo and B. M. Gaensler, (San Francisco:ASP), p. 39, 2004.
- [32] M. Morini, MNRAS, 303, 495, 1983.
- [33] A. G. Muslimov & A. K. Harding, ApJ, 588, 430, 2003.
- [34] A. G. Muslimov & A. K. Harding, ApJ, 606, 1143, 2004.
- [35] A. G. Muslimov & A. K. Harding, in preparation, 2005.
- [36] A. G. Muslimov & A. I. Tsygan, MNRAS, 255, 61, 1992.
- [37] D. Page, ApJ, 442, 273, 1995.
- [38] Radhakrishnan & Cooke, ApL, 3, 225, 1969.
- [39] J. Rankin, ApJ, 405, 285, 1993.
- [40] H. Riffert & P. Meszaros, ApJ, 325, 207, 1988.
- [41] R. W. Romani, ApJ, 470, 469, 1986.
- [42] R. W. Romani & I. A. Yadigaroglu, ApJ, 438, 314, 1995.
- [43] Yu. P. Shitov, Soviet Astron. 27, 314, 1983.
- [44] F. G. Smith, MNRAS, 219, 729, 1986.
- [45] J. Takata, S. Shibata & K. Hirotani, MNRAS, 354, 1120, 2004.
- [46] Thompson, D. J. 2001, in *High Energy Gamma-Ray Astronomy*, American Institute of Physics (AIP), vol 558, Ed. Felix A. Aharonian and Heinz J. Vlk. (AIP, Melville, NY), p. 103.
- [47] C. Venter & O. C. DeJager, ApJ, 619, L167, 2005.
- [48] I. Wasserman & S. L. Shapiro, ApJ, 265, 1036, 1983.
- [49] I. A. Yadigaroglu, Ph.D. Thesis, Stanford University, 1997.